AGU PUBLICATIONS

Water Resources Research

RESEARCH ARTICLE
10.1002/2015WR017348

# Use of ADCPs for suspended sediment transport monitoring: An empirical approach

**J. G. Venditti[1], M. Church[2], M. E. Attard[1], and D. Haught[1]**

[1]Department of Geography, Simon Fraser University, Burnaby, British Columbia, Canada, [2]Department of Geography, The University of British Columbia, Vancouver, British Columbia, Canada

**Key Points:**
- ADCP calibrations for suspended sediment conform with acoustic theory
- Sand and silt both correlate with acoustic backscatter
- Auxiliary relations extend results to full-channel transport

**Correspondence to:**
M. Church,
mchurch@geog.ubc.ca

**Citation:**
Venditti, J. G., M. Church, M. E. Attard, and D. Haught (2016), Use of ADCPs for suspended sediment transport monitoring: An empirical approach, *Water Resour. Res.*, *52*, 2715–2736, doi:10.1002/2015WR017348.

Received 3 APR 2015
Accepted 7 MAR 2016
Accepted article online 12 MAR 2016
Published online 8 APR 2016



**Abstract** A horizontally mounted 300 kHz acoustic Doppler current profiler was deployed in Fraser River at Mission, British Columbia, to test its capability to detect size-classified concentration of suspended sediment. Bottle samples in-beam provide a direct calibration of the hADCP signals. We also deployed a 600 kHz vertically mounted ADCP from a boat in combination with bottle samples. Fraser River at Mission is 525 m wide with moderate suspended sediment concentration (up to 350 mg $L^{-1}$ in our measurements, mostly silt), and a modest sand load only at high flows. We use an entirely empirical approach to calculate the sediment load using ADCPs to test the reliability of acoustic methods when assumptions embedded in the sonar equation about the relation between suspended sediment size and concentration, and acoustic signals are violated. vADCP calibration using matched individual bottle samples and acoustic backscatter departed from the expected theoretical relation. Calibration using depth-averaged sediment concentration and acoustic backscatter more closely matched theoretical expectations, but varied through the season. hADCP calibrations conformed with theoretical expectations and did not exhibit seasonal variation. Silt and sand were successfully discriminated; however, silt dominates the correlations. We found no coherent relation between acoustic attenuation and silt concentration. In-beam results are extended by correlation to estimate mean sediment concentration and total suspended flux in the entire channel: this auxiliary correlation cancels any calibration bias and permits monitoring of size-classified suspended sediment in absence of detailed information of sediment grain-size distribution.

## 1. Introduction

Suspended sediment concentration in water bodies has traditionally been determined by bottle or pump sampling and subsequent laboratory analysis of filtered solids content. The physical sample provides a definitive indication of sediment concentration and size, but its acquisition and analysis are laborious procedures that do not permit high-resolution measurement, either spatially or temporally (see *Gray and Landers* [2013] for a recent review of traditional measurements based on the widely adopted practices of the United States Geological Survey). Automatic pump samplers may improve temporal resolution to some degree, but do not improve important spatial resolution, and still require substantial attention and labor.

The application of suspended sediment rating curves may to some extent overcome the temporal limitation of measurements, but suspended sediment concentration varies substantially with variable sediment supply to the water body so that rating curves are subject to significant errors [*Walling*, 1977]. Optical instruments have been developed to continuously sense suspended sediment concentration at-a-point by measuring light transmission or backscatter, but the response depends on grain size and is a nonlinear function of concentration [*Downing*, 1983]. More problematic is that the sensing elements of these instruments are subject to fouling, necessitating frequent maintenance [*Hamilton et al.*, 1998], often yielding only a few days' data in biologically productive environments [*Gartner*, 2004].

Over the past two decades, the development of hydroacoustic instruments (Acoustic Doppler Current Profilers, hereafter "ADCP") for measuring water velocity by detecting acoustic energy backscattered from particulate matter in the water column has permitted the detection of suspended sediment with very high temporal resolution and, potentially, high spatial resolution. It is also a substantial advantage for sediment flux estimation that these instruments can return data of both velocity and sediment concentration. The theory that underlies the application of acoustic transducers to measure suspended sediment is summarized by *Thorne and Hanes* [2002] and, more recently, by *Thorne and Hurther* [2014].

Combining equations given in *Thorne and Hanes* [2002], the foundational sonar equation can be written in logarithmic form as

$$RL = SL - (SP + AT) + 10\log_{10}\left\{\frac{M}{\rho_s}\right\} + 10\log_{10}\left\{ff^2\frac{3}{16}\frac{\tau c}{a_s}\left[\frac{0.96}{ka_t}\right]^2\right\} \quad (1)$$

wherein $RL$ is reverberation level (i.e., the signal recorded by the ADCP), $SL$ is source level (outgoing signal), $SP$ is the beam spreading loss, $AT$ is the signal attenuation loss, $M$ is sediment mass concentration, and $\rho_s$ is sediment density. The last term is the target strength, $TS$, which depends on $ff$, the form function, $\tau c$, the pulse length (pulse time $\times$ pulse celerity), $a_s$, the sediment grain radius, $k$, the acoustic wave number, and $a_t$, the transducer radius. The form function represents the cross section of the particle that is backscattering acoustic energy, which varies with particle diameter and shape. Combining $SL$, which is constant for a transducer, and the target strength term in equation (1), which is a constant *for a given particle size* and ADCP, into a constant $K_t$, the sonar equation becomes, with some rearrangement

$$\log_{10}\left\{\frac{M}{\rho_s}\right\} = 0.1(RL + 2TL) - 0.1K_t \quad (2)$$

with $2TL = SP + AT$ denoting the two-way transmission loss [*Wright et al.*, 2010]. The term $(RL + 2TL)$ is the adjusted backscatter measured by the transducer, corrected for transmission losses along the beam path. Linear regression between backscatter and the logarithm of volumetric sediment concentration should, then, theoretically yield a slope of 0.1 and an intercept of $0.1K_t$ [*Gartner*, 2004; *Wright et al.*, 2010]. Correction of $RL$ (which is what is measured by the transducer) for two-way transmission losses can be estimated from

$$2TL = 20\log_{10}(r) + 2\alpha_f r + 2\alpha_s r \quad (3)$$

wherein $\alpha_f$ and $\alpha_s$ are the fluid and sediment attenuation coefficients [*Wright et al.*, 2010] and $r$ is the distance from the transducer, with further correction in the near field. Theoretical expressions for the attenuation coefficients involve infinite series, so they are commonly estimated from empirical relations (see review in *Flammer* [1962]; also our equations (7) and (8)).

There has been extensive research-focused application of the sonar equation and acoustic signals to predict mass concentration and grain size of particle suspensions: reviews of early work are given by *Hay and Sheng* [1992] and by *Thorne and Hanes* [2002]. Much of this research has been laboratory based and has provided the basis to invert acoustic signals to estimate suspended sediment concentration and grain size for sand-sized particles [cf. *Hay*, 1991; *Hay and Sheng*, 1992; *Crawford and Hay*, 1993; *Thorne et al.*, 1993; *Thorne and Hardcastle*, 1997; *Thosteson and Hanes*, 1998; *Thorne and Hanes*, 2002; *Thorne and Buckingham*, 2004; *Moate and Thorne*, 2009, 2013; *Moore and Hay*, 2009; *Thorne et al.*, 2010; *MacDonald et al.*, 2013]. The primary focus of this work has been to define expressions for the scattering properties of the particle and the attenuation characteristics of the scatterers. It emerges—as is implicit in equation (1)—that both acoustic scatterance and attenuation depend on sediment size and mass concentration of the scatterers. Without prior knowledge of those properties, inversions for sediment concentration from acoustic backscatter may remain unbiased only for suspensions of fixed size distribution and uniform concentration.

Accordingly, early applications of acoustics for sensing sediment, mostly in ocean and estuarine environments (summarized by *Hay and Sheng* [1992] and *Thorne and Hanes* [2002]), used custom-designed instruments operating at multiple frequencies of order 1 mHz to obtain observations of suspended sediment concentration over short ranges within which sediment properties remained essentially constant. The more recent proliferation of commercially available, single-frequency, downward-looking ADCPs (vADCPs) has extended the range of observations that can be obtained to the whole water column. vADCPs are increasingly used in examinations of sediment dynamics in estuaries [e.g., *Thevenot and Kraus*, 1993; *Hill et al.*, 2003; *Gartner*, 2004; *Wall et al.*, 2006, 2008; *Wargo and Styles*, 2007; *Defendi et al.*, 2010; *Sassi et al.*, 2012; *Bradley et al.*, 2013] and rivers [e.g., *Reichel and Nachtnebel*, 1994; *Holdaway et al.*, 1999; *Filizola and Guyot*, 2004; *Kostaschuk et al.*, 2005; *Jugaru Tiron et al.*, 2009; *Szupiany et al.*, 2009; *Shugar et al.*, 2010; *Sassi et al.*, 2013a,b; *Guerrero et al.*, 2013; *Tiron Duţu et al.*, 2014]. In these environments, sediment properties vary significantly.

Conventional vADCPs still require supervised deployment, which limits their use as monitoring instruments, though much useful information might be recovered in the course of routine hydrometric measurements. However, the development of horizontally mounted ADCPs (hADCPs) for velocity-index discharge measurements permits a temporally continuous and spatially extended index measurement to be gained of passing suspended sediment in rivers without continuous supervision. Arrays of hADCPs to measure fluvial suspended sediment concentration in a river cross section (or portion thereof) have been deployed by *Topping et al*. [2007] in the Colorado River [see also *Wright et al*., 2010], by *Moore et al*. [2011] in the Rhône, Saône, and Isère Rivers (France) [see also *Moore et al*., 2013], and by *Wood and Teasdale* [2013] in the Clearwater and Snake Rivers (USA). *Topping et al*. [2007], building on the work of *Flammer* [1962], identified two acoustic size classes: a finer size class (silt/clay), in which increasing concentration results in greater attenuation of sound due to viscous losses (see *Moore et al*. [2013] for sample attenuation curves), and a coarser size class, corresponding to sand, that results in increased backscattering of sound. They correlated the acoustic signals against velocity-weighted, cross-section-averaged sediment concentrations derived from depth-integrated sampling. Correlations were developed between the silt-clay concentrations and the hADCP signal attenuation and between sand and the backscatter, yielding predictions of sediment concentration specific to each grain-size class and opening the way to obtain size-classified information from a single instrument of fixed frequency. But earlier investigators have successfully correlated silt concentration with acoustic backscatter [e.g., *Hoitink and Hoekstra*, 2005; see also *Wood and Teasdale*, 2013].

Most of the exercises with vADCPs have sought correlations between acoustic backscatter and depth-integrated suspended sediment concentration (that is, profile-average SSC), but *Wall et al*. [2006] correlated the signals from individual ADCP bins (essentially, fixed depths) with collocated point-integrated SSC, using the average of four ADCP beams to gain a measure of local spatial averaging. *Sassi et al*. [2012, 2013b] also employed point-integrated samples. They used the measured backscatter profile and the samples to calculate sediment scattering attenuation due to mass concentration. Viscous attenuation and scattering attenuation due to sediment size variation along the acoustic beam were assumed to be negligible. Among hADCP users, *Topping et al*. [2007] and *Wood and Teasdale* [2013] sought their results by correlating observed backscatter with the depth-integrated mean sediment concentration in the river. *Moore et al*. [2011] correlated hADCP signal returns with the data of an optical backscatter instrument; direct sediment samples were taken to calibrate the optical instrument and for grain-size confirmation. In this case, then, one index signal was used to investigate the consistency of another.

The field applications described above come face to face with constraints posed by the sonar equation, which generally limit the possibility to obtain theoretically strict estimates of suspended sediment concentration and size by acoustic means [*Sassi et al*., 2012; *Hanes*, 2013]. While equation (1) is specified for an individual grain size, in a natural water column, one always senses a range of sizes which, furthermore, usually vary along the beam vertically and, potentially, across stream. Correlation of the acoustic signal with spatially integrated measures of SSC directly addresses the objective of measuring suspended sediment concentration but does not constitute a critical test of acoustic principles as the basis for the method. It is simply an empirical correlation based on the sonar principle and, since the instruments view only a restricted sample of the water column, its success relies on there being a consistent distribution of suspended sediment throughout the water body. Most prior investigations in natural water bodies have assumed a correlation between acoustic backscatter and some bulk measure of sediment concentration without critical examination of these assumptions.

There has not yet been a direct comparison of primary hADCP signal returns with collocated conventional bottle or pump sampling techniques and, to our knowledge, only the work of *Wall et al*. [2006] and *Sassi et al*. [2012] has achieved this standard of investigation for vADCPs. In this paper, we seek to advance the basis for routine monitoring of suspended sediment by directly calibrating the ADCPs using physical sediment samples taken directly in the beam of the instrument to provide a test of the robustness of empirical correlations based on the sonar equation. Further, we extend our observations to study the correlation between both vADCP and hADCP observations and measures of mean sediment concentration in the entire water column to predict sediment flux in the river.

Many of the rivers in which ADCPs have been deployed to monitor sediment fluxes are characterized by high sediment loads. The Colorado River site has sediment concentrations up to 20,000 mg $L^{-1}$, of which 3000 mg $L^{-1}$ is sand [*Topping et al*., 2007] (hADCP). The sites in the French Rivers are also characterized by

high sediment concentrations, up to 8000 mg $L^{-1}$ during high flows (hADCP; S. A. Moore, Monitoring flow and fluxes of suspended sediment in rivers using side-looking acoustic Doppler current profilers, unpublished PhD dissertation, University of Grenoble, 2011) most of which is silt-clay-sized sediment. In contrast, in the Hudson estuary [*Wall et al*., 2006, 2008] (vADCP), SSC did not exceed 100 mg $L^{-1}$, and in the Clearwater and Snake Rivers [*Wood and Teasdale*, 2013] (hADCP) concentrations remained below 180 and 500 mg $L^{-1}$, respectively. In these conditions, sediment-associated beam attenuation may not pose a significant problem. We deployed a shore-mounted 300 kHz hADCP in Fraser River at Mission, British Columbia (Figure 1), where sediment concentrations are intermediate between the extremes previously studied, approaching but rarely exceeding 1000 mg $L^{-1}$ while our measurements did not exceed 350 mg $L^{-1}$. Although a significant portion during high flows is sand, the suspended sediment load is dominantly silt [*McLean et al*., 1999].

Fraser River is ~525 m wide at Mission, so we chose a 300 kHz instrument for its superior range. We also made periodic observations with a boat-mounted 600 kHz vADCP. Our work is distinguished from the work with hADCPs of *Topping et al*. [2007], Moore (unpublished PhD dissertation, 2011), and *Wood and Teasdale* [2013], in that we made direct measurements of sediment concentration and grain size using conventional bottle sampling in the acoustic beam. This allowed us to develop a formal calibration of the ADCP instrument signals with reference to the sonar equation in the manner of *Wall et al*. [2006, 2008] for a vADCP. The goal of our work is to determine whether we can calculate suspended sediment fluxes accurately in a river without embedding the analysis in all the assumptions implicit in the sonar equation. We seek to answer the following questions: (i) How do field-based calibrations of ADCP signals against conventional bottle-sample measurements of SSC compare to sonar theory? (ii) What is the most appropriate methodology to calculate sediment loads from a calibrated ADCP in light of the limitations posed by sonar theory? We thereby hope to critically test an empirical basis for hydroacoustic detection of suspended sediment in rivers and estuaries, where significant gradients in suspended sediment properties are the rule. As noted, we extend our results to present consistent means to estimate the sediment flux in the entire channel.

## 2. Methods

### 2.1. Study Site

Fraser River at Mission drains 228,000 $km^2$ of the humid British Columbia Coast Mountains, subhumid interior plateaux, and the Columbia and Rocky Mountains. The annual hydrograph is dominated by the spring snowmelt freshet, with high flows occurring from late May until early July, and an extended recession through the rest of the year with minor rises due to autumn rainstorms. One has, in effect, a single event hydrograph at annual scale. Mean annual flood is 9790 $m^3\ s^{-1}$. The sediment load, averaging $17 \times 10^6$ tonnes per annum (on the basis of 1966–1986 measurements by the Water Survey of Canada (WSC)), is composed mainly of fine sand (<180 μm), silt and subordinate clay derived from the erosion of Quaternary sediments along the length of the river. On average, 18% of the annual suspended sediment load is sand > 180 μm [*McLean et al*., 1999], all of which is transported during the freshet. The river bed at Mission is composed of sand (median diameter ~380 μm) [*Attard et al*., 2014] that contributes intermittently suspended material and a bedload component. The bed is relatively flat at the study site but is covered with dunes in the upstream reach with amplitudes of order 1 m during flood.

The observation section is located 240 m upstream from the Mission water level gauge (WSC Stn. 08MH024) and the Mission railway bridge (Figure 1), from which the WSC measurements were taken. River width here at mean annual flood is 540 m, declining to 520 m at mean flow stage. The river is tidally influenced at this point (85 km from the mouth at Sand Heads): during freshet the tidal variation is only a few centimeters but it may exceed one meter during winter high tides. The effect on velocity, however, remains significant at the highest flows as the river is subject to a backwater effect on rising tide. This semidiurnal variation is an additional reason to establish a system of automated continuous recording of suspended sediment concentration and flux. The seasonally reliable variation in flow and suspended sediment content makes the site ideal for exploratory investigation of acoustic instruments for detection of suspended sediment.

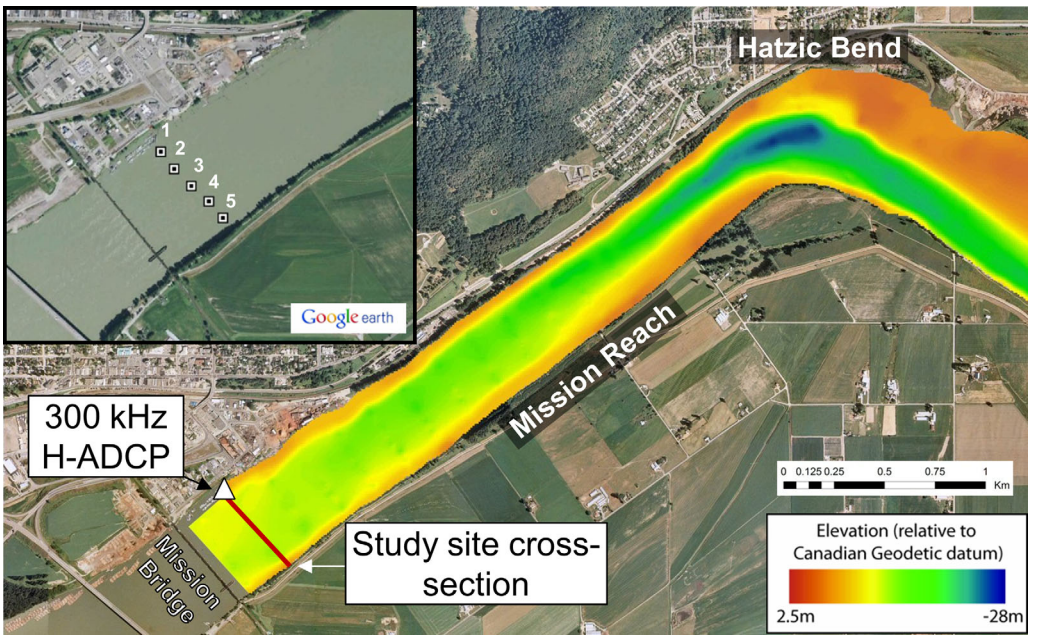


**Figure 1.** Bed topography of Mission Reach and Hatzic bend showing the location of the 300 kHz hADCP and the study cross section. Inset shows locations of bottle sampling and 600 kHz vertical ADCP profiles (numbered 1–5). Bed topography is from Public Works Canada cross sections measured every 100 m along the channel in 2008. Main imagery from 1995 airphotos. Inset imagery from Google Earth accessed 6 July 2013.

### 2.2. Instrument Deployment

A 300 kHz (exact frequency 307.2 kHz) Teledyne RD ChannelMaster® hADCP was mounted on the Mission Harbour dock (Figure 1) on the right bank of the river. It was fixed at −0.9 m geodetic datum and tilted down at 1.2° in order to sample the full water column and to avoid interference from the water surface. The hADCP has a beam spread of 2.2°; the consequent beam projection is shown in Figure 2. The instrument was set to collect data in 128 bins each of 2 m width so that, with a 3 m blanking distance, its theoretical range extended 259 m into the channel—that is, about halfway across. Data were downloaded at approximately 0.2 Hz to a computer mounted on the dock. Data collection commenced on 12 April 2010 and was continuous until 19 August except for a power outage on 26 June. From 19 August until 3 November, data were collected intermittently since the shortening days did not permit the solar panels that powered the installation to generate sufficient energy for continuous operation.

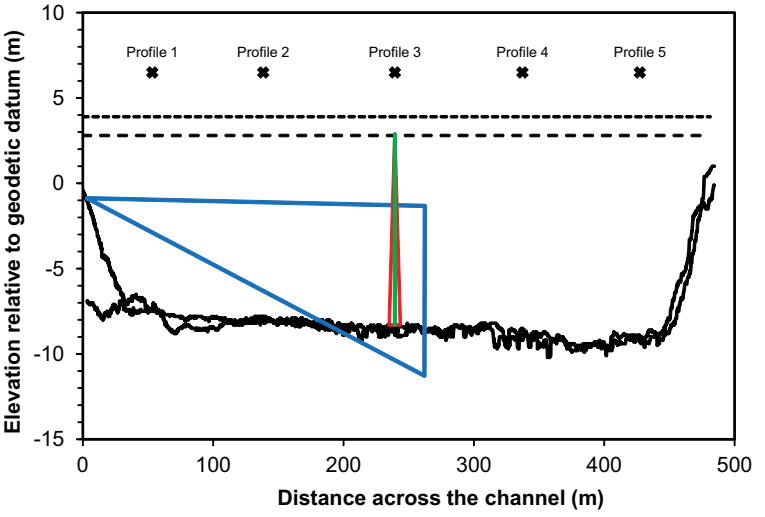


**Figure 2.** Ensonified areas of the 300 kHz horizontal ADCP (blue) and the 600 kHz vertical ADCP (red is all four beams and green is the forward looking beam #3). Solid black lines are the bed topography immediately upstream and downstream surveyed in 2008 by Public Works Canada. Crosses mark the positions of the bottle-sampled profiles and vADCP observations. The long dashed line is the water level at Mission when the discharge at Hope was ~5000 $m^3/s$ (~6060 $m^3/s$ at Mission) in 2010. The short dashed line is the water level at Mission during the peak 2010 discharge (~7500 $m^3/s$).

A 600 kHz (exact frequency 614.4 kHz) Teledyne RD Workhorse Rio Grande® vADCP was deployed from a 6 m launch to collect vertical profiles of velocity and suspended sediment concentration at five positions across the channel (Figure 2). Data were recorded at approximately 1 Hz to an onboard computer. A Trimble GPS Rover operated in RTK mode was used for positioning. Sampling dates are listed in Figure 4.

Bottle samples were taken in the beam of the hADCP at eight fixed distances from the instrument between 27.5 and 300 m with a P63 suspended sediment sampler. The P63 [*Gray and Landers*, 2013] is a point-integrating sampler that collects an isokinetic sample in a 950 mL bottle. Sampling times were varied to achieve samples that typically varied from 700 to 850 mL. Bottle samples were also collected at the five vADCP profile positions for calibration purposes and to calculate the total sediment flux in the channel independently of the ADCP observations (see *Attard et al*. [2014] for analysis of bottle sampled sediment flux). The P63 was deployed from the opposite side of the launch (separation from the acoustic signal approximately 2 m) and samples were taken at 0.1, 0.2, 0.4, 0.6, and 0.8 of full depth, with minor variations on 16 April (four positions in profile) and 28 June (Profile 5 not collected) due to instrument failures.

### 2.3. Data Processing

The use of hydroacoustic instruments to measure suspended sediment is based on the sonar equation in the form of equation (2), extended by an empirical relation between suspended sediment concentration and acoustic backscatter adjusted for two-way transmission losses. ADCPs return a measure of backscatter (*RL*) as the echo intensity (*EI*) in counts, which is converted to *RL* in decibel units as:

$$RL = sf \times EI \tag{4}$$

in which *sf* is an instrument-specific scale factor. The measured backscatter is corrected for two-way transmission losses associated with fluid attenuation by applying the sonar equation [*Urick*, 1975] to calculate the fluid-corrected backscatter (*FCB*) from

$$FCB = RL + 20\log_{10}(r) + 2\alpha_f \tag{5}$$

wherein $r$ is distance along the acoustic beam. This has the effect of replacing the backscatter lost to fluid attenuation with distance from the transducer. In the "near field," the second term becomes $20log_{10}(r\psi)$ wherein $\psi$ is an additional correction. *Wall et al*. [2006] determined that this factor makes of order 1% difference to the final result, so we have ignored it. We have also ignored several instrument-specific constants because they affect only the magnitude of the signal, but not its relative variability [cf. *Deines*, 1999; *Sassi et al*., 2012]. The water absorption coefficient, $\alpha_f$, is computed [*Schulkin and Marsh*, 1962] for zero salinity from

$$\alpha_f = 8.686 \times 3.38 \times 10^{-6} \frac{f^2}{f_T} \tag{6a}$$

$$f_T = 21.9 \times 10^{\left(6 - \frac{1520}{T+273}\right)} \tag{6b}$$

wherein $f$ is the frequency of the ADCP and $T$ is the water temperature in degrees Celsius.

In flows with high sediment concentrations, corrections for two-way transmissions losses associated with sediment in suspension may also be needed. This can be accomplished by calculating the sediment corrected backscatter as

$$SCB = FCB + 2\alpha_s r \tag{7}$$

where $\alpha_s$ is a sediment attenuation coefficient which can be calculated from theory [*Hay*, 1991], semitheoretically [e.g., *Sassi et al*., 2012] or empirically [*Topping et al*., 2007; *Wright et al*., 2010]. This correction has the effect of replacing the backscatter lost to viscous and scattering attenuation with distance from the transducer. The theoretically strict calculation requires the grain-size distribution and mass concentration of particles in suspension [e.g., *Moore et al*., 2013; *Moate and Thorne*, 2013]. If the size or mass concentration varies along the acoustic beam or through time, that variation must also be known. The consequent need for continuous physical sampling would defeat the purpose of the acoustic observations in a long-term monitoring program.

*Sassi et al*. [2012] introduced a semitheoretical method to account for attenuation that simplifies the data requirements somewhat by requiring only mass concentration near the transducer, where sediment

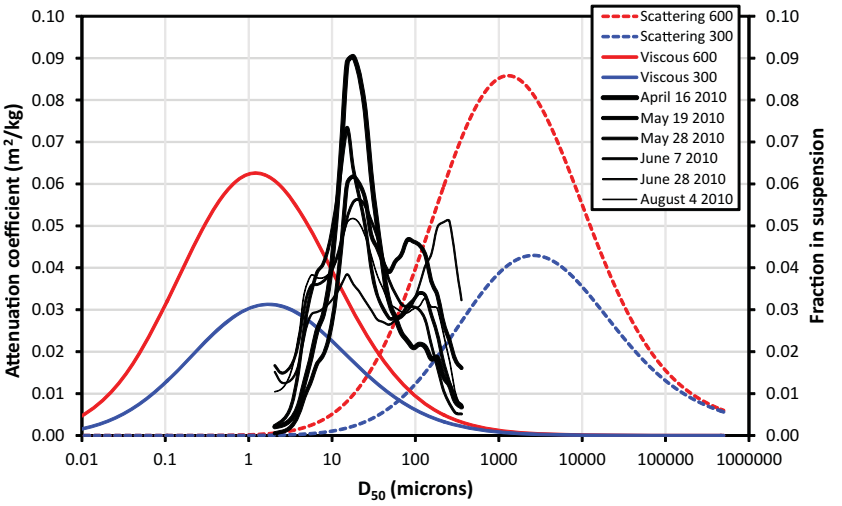


**Figure 3.** Viscous and scattering attenuation coefficients plotted as a function of median grain size for the 300 and 600 kHz transducers. Also plotted are the grain-size distributions from each sampling campaign for Profile 3 at 0.6d.

attenuation is assumed to be negligible, and somewhere else along the acoustic beam where scattering attenuation is assumed to occur due to the gradient in mass concentration. Viscous attenuation by sediment and scattering attenuation that may occur due to a gradient in sediment size is ignored. This method cannot be successfully applied to our data because viscous sediment attenuation is not negligible for the combination of suspended sediment sizes in the Fraser and our acoustic frequencies (Figure 3). Furthermore, there is a substantial grain-size gradient (see below) that can contribute to the scattering attenuation.

An empirical approach is somewhat simpler in that $\alpha_s$ is calculated as

$$\alpha_s = -\frac{1}{2} S_{FCB,r} \tag{8}$$

where $S_{FCB,r}$ is the slope of the least squares linear regression between *FCB* and *r* [*Topping et al*., 2007; *Wright et al*., 2010] (equation (8) is the derivative, *d*/*dr*, of equation (7), under the assumption that sediment concentration is independent of *r*). However, its calculation assumes spatially uniform sediment properties such that $S_{FCB,r}$ is negative. In the presence of physical gradients in size and mass concentration, $S_{FCB,r}$ depends on sediment attenuation and those gradients. The requirement for uniform mass concentration and sediment properties along the acoustic beam can be coincidentally met in some hADCP deployments, but rarely in vADCP deployments.

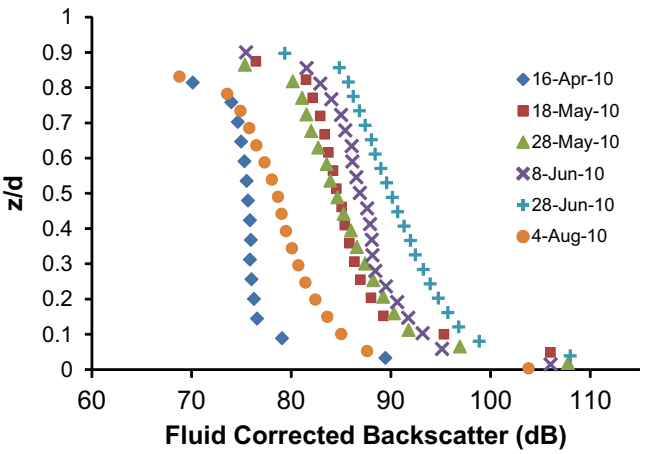


**Figure 4.** Typical vertical profiles of fluid corrected backscatter from the 600 kHz vADCP at Profile 3. Profile 4 is substituted for Profile 3 on 16 April 2010 because of an instrument failure.

We implemented the empirical sediment correction method for the hADCP because the underlying assumptions could be met. A fortunate consequence of selecting a 300 kHz instrument for maximum range is that the instrument has minimum sensitivity to both viscous and scattering sediment attenuation for sediments suspended in Fraser River (Figure 3). This means that the sediment corrections are small. Some care needs to be taken in calculating $S_{FCB,r}$ because obstructions within the ensonified volume of flow and signal decay beyond the specified operating range of the ADCP will affect the *FCB*-*r* relation, but

not necessarily the recorded velocity. This correction reduced hADCP backscatter to a common integral value, obviating the possibility to make bin-by-bin estimates of sediment concentration.

Application of this empirical method to correct the vADCP data is not possible due to the gradients in mass concentration and grain size. Removing the vertical gradient in the same manner as the hADCP would have the effect of rotating the profile about the first point not affected by near-field effects. *SCB* would be less than the measured backscatter. We applied the *Sassi et al*. [2012] method to our 600 kHz records and found negative values of $\alpha_s$ along the entire profile, so we did not pursue this method further. We therefore focus further analysis on the bin-by-bin and depth-averaged *FCB*. Like the 300 kHz instrument, the 600 kHz vADCP has minimum sensitivity to both viscous and scattering attenuation for the majority of suspended sediments in the Fraser River (Figure 3). This suggests that the necessary correction is small and can probably be ignored, an assumption we can test by comparison of our *FCB* observations with theoretical expectations.

In order to calculate suspended sediment concentration (*SSC*) from *FCB*, we used the following relation, due to *Gartner* [2004]:

$$SSC = 10^{(a*FCB+b)} \tag{9a}$$

wherein *a* and *b* are the slope and intercept of a least squares regression, respectively. We investigated the separate sand and silt-clay calibrations with *FCB* and investigated the hADCP calibrations with *SSC* computed from *SCB* as

$$SSC = 10^{(a*SCB+b)} \tag{9b}$$

*Topping et al*. [2007] and *Wright et al*. [2010] have argued that *FCB* can be related to total sediment concentration, *SCB* to sand concentration, and silt-clay concentrations to $\alpha_s$. We also studied the correlation between silt-clay concentration and $\alpha_s$ but, finding no significant result, we did not pursue this relation.

Data were correlated using linear least squares under logarithmic transformation of *SSC*. Because residuals are not normally distributed, back-transform bias was eliminated to obtain equations (9) using the "smearing" method [*Duan*, 1983; *Newman*, 1993]. The underlying calibrations were obtained as reduced major axis functional relations, which assume that the error ratio of the variables is equal to the ratio of their sums of squared departures from the mean, and is the maximum likelihood estimate of the error ratio when it is in fact unknown [see *Mark and Church*, 1977].

## 3. ADCP Calibrations

### 3.1. The 600 kHz vADCP

Figure 4 displays fluid-corrected backscatter from the vADCP in the center of the channel. Backscatter increased toward the bed, as expected, and the backscatter intensity varied through the season in concert with flow and suspended sediment concentration. Calibrations were developed between the variously corrected acoustic signals and sampled sediment mass concentration for the total and component concentrations. In the calibration exercise, vADCP data immediately adjacent to the surface and the bed that were obviously perturbed by the presence of the boundaries were ignored. This entailed deleting data above and below the infection points in Figure 4.

The most direct relation between the acoustic signal and *SSC* is obtained by correlation between the physical sample and the acoustic signal from the vADCP profile bin in (or very near) which the physical sediment sample was collected (bin-by-bin calibration), which we obtain for *FCB*. We also obtained the correlation between the depth-averaged *FCB* and *SSC*—"indirect" results, but convenient for prediction of profile-average *SSC*. Figure 5 displays bin-by-bin and depth-averaged calibrations. The bin-by-bin results are based on the instrument signal observed in the profile bin at the depth at which the physical sample was taken, but there remains the 2 m lateral distance between the two observations. All samples were used, normally yielding five calibration points per profile.

The depth-averaged SSC from bottle sampling was calculated as

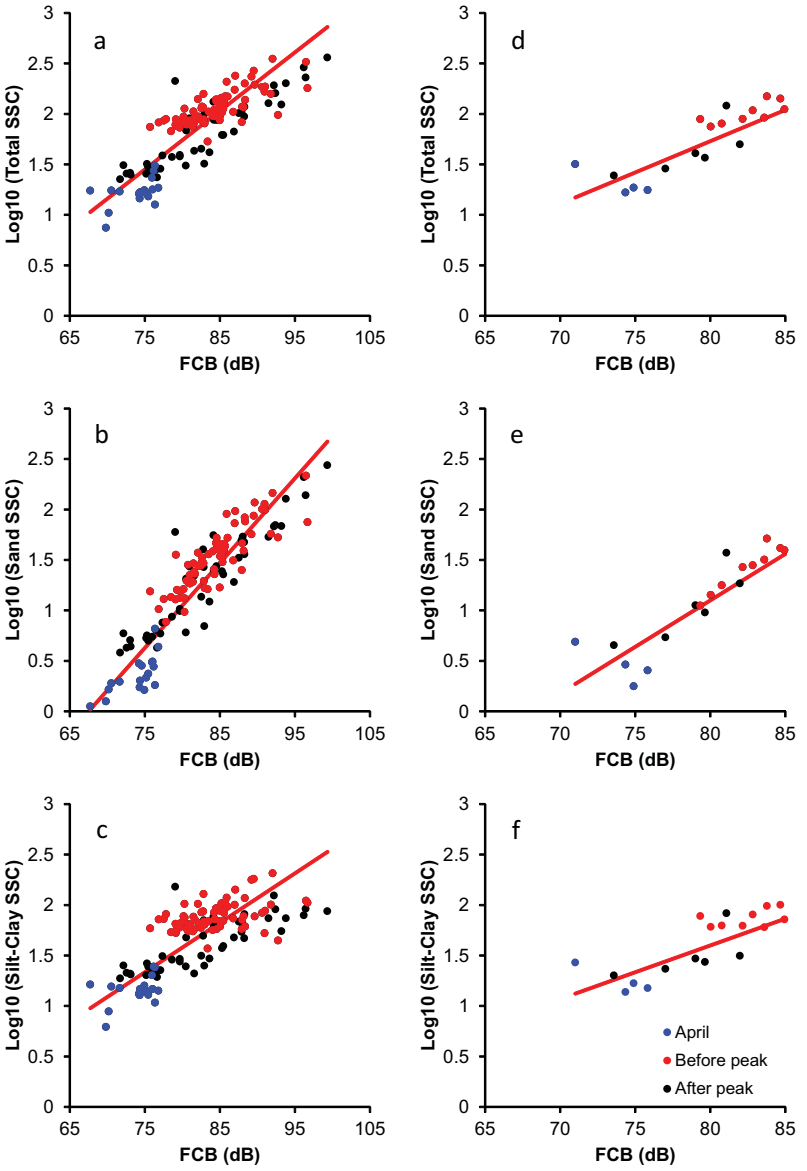


**Figure 5.** (a–c) Bin-by-bin calibration curves with fluid corrected backscatter (FCB) and (d–f) same for depth-averaged calibration curves for the vADCP: Figures 5a and 5d for total suspended sediment concentration, Figures 5b and 5e are for suspended sand concentration, and Figures 5c and 5f are for silt-clay concentration. Red lines are reduced major axis functional relations [*Mark and Church*, 1977].

$$<SSC> = \sum c_i d_i u_i / \sum d_i u_i \tag{10}$$

in which $<SSC>$ is the profile-averaged SSC (angle brackets indicate a depth-average), $c_i$ is a sample value, $d_i$ is the height of the water column that the sample represents, and $u_i$ is the velocity from the corresponding ADCP bin, representing the mean velocity for the corresponding depth range. The depth-averaged *SSC* from the vADCP is calculated in similar fashion with $c_i$ derived from the ADCP calibration.

Table 1 reports the calibration statistics, which are highly significant for total suspended sediment concentration and for both sand and silt-clay components. The gradients of the sand relations fall closest to the theoretical expectation (0.1), but the gradients for the full GSD and for silt-clay fall well below that value. The depth-averaged calibrations are somewhat improved (Table 1), presumably because the averaging process reduces the effect of varying particle size scatterance. The intercepts of the calibration equations imply a constant, $K_t$, near 20 for the full GSD, near 12 for silt/clay and 50 for the sand correlation (variation of the value being expected

**Table 1.** Summary of vADCP Calibrations

| | | Log Regression | | | | | | Functional Relation | | |
|---|---|---|---|---|---|---|---|---|---|---|
| | *n* | Slope (*a*) | Intercept (*b*) | $R^2$ | *P* Value[a] | SEE[b] | Back-Transform Correction | Slope (*a*) | Intercept (*b*) | Confidence Range of Slope[c] |
| *Bin × Bin: FCB* | | | | | | | | | | |
| Full GSD | 134 | 0.049 | −2.19 | 0.72 | $1.06 \times 10^{-36}$ | 0.195 | 1.10 | 0.058 | −2.90 | 0.052–0.064 |
| Sand | 134 | 0.077 | −5.05 | 0.83 | $1.90 \times 10^{-52}$ | 0.222 | 1.14 | 0.084 | −5.67 | 0.078–0.091 |
| Silt-clay | 134 | 0.036 | −1.26 | 0.54 | $8.50 \times 10^{-24}$ | 0.211 | 1.12 | 0.049 | −2.34 | 0.041–0.057 |
| *Avge: FCB* | | | | | | | | | | |
| Full GSD | 28 | 0.054 | −2.57 | 0.76 | $1.89 \times 10^{-09}$ | 0.164 | 1.07 | 0.062 | −3.23 | 0.048–0.076 |
| Sand | 28 | 0.085[d] | −5.68 | 0.85 | $2.46 \times 10^{-12}$ | 0.189 | 1.09 | 0.092[d] | −6.26 | 0.077–0.107 |
| Silt-clay | 28 | 0.041 | −1.68 | 0.61 | $9.92 \times 10^{-07}$ | 0.178 | 1.08 | 0.053 | −2.64 | 0.036–0.070 |

[a]For regression slope.
[b]Standard error of estimate: $\log_{10}$ units.
[c]The 95% range.
[d]Not significantly different than 0.100 ($p = 0.05$).

because it depends, amongst other factors, on the "effective grain size" of the sediment scatterers). It is clear that the silt-clay fraction dominates the total GSD of suspended sediment in Fraser River (Figure 6), accounting for the similarity of the calibrations for total GSD and for silt-clay.

We find, however, that the overall calibrations displayed above are not stable. Figure 7 shows that results from an individual sampling may remain biased. Indeed, dividing the data into subsets for the rising limb and falling limb of the hydrograph leads to distinct clusters of data (Figure 5) and to calibration equations with significantly different slopes (0.062 versus 0.041; $p < 0.05$ for total *SSC* with *FCB* bin-by-bin). Before the freshet peak, suspended sediment concentration appears to respond with more sensitivity than after the peak. But if, instead, we group the low flow observations of 16 April (before the commencement of the freshet, when total suspended sediment concentration was very low (values 10–30 mg $L^{-1}$) with the post-freshet observations, we find two equations with equivalent slope but different intercepts, implying a systematically changed grain size. The presence/absence of a significant suspended sand component (Figure 3) may account for the shift. The depth-averaged results appear to be more stable in this regard.

### 3.2. The 300 kHz Horizontal ADCP

Figure 8a shows the season-long cross-stream backscatter signal (water corrected) recovered from the hADCP, which follows the seasonal pattern of streamflow, as does sediment concentration. Figure 8b shows in detail the raw and corrected signals for 28 June (the peak flow day). Both parts of the figure exhibit the same unexpected feature: signal strength declines as expected out to 60 m, but then increases to 130 m before beginning to decrease again. The signal also shows increased local variation beyond 60 m. We interpret these features to indicate that the beam has encountered some unusual interference beyond 60 m. Figure 2 shows that bed interference should be encountered only near 180 m and that water surface interference should not occur. The bed is probably the source of interference in view of transducer side-lobe effects but we remain uncertain—in any event, the signal appears to be spurious beyond 60 m. This outcome compromises hADCP in-beam calibration measurements beyond that distance, consequently we confine attention to a beam-averaged calibration covering the first 60 m. In this sector, relatively quiet water carries silt and fine sand with limited size variation over the season and in the vertical (Figure 9), and a small range in concentration (Figure 10), making the accessible sampling volume relatively ideal for consistent hADCP sediment detection. (*Buschman et al.* [2012] have previously described low cross-sectional variation in suspended sediment concentration in a silt-clay dominated river.)

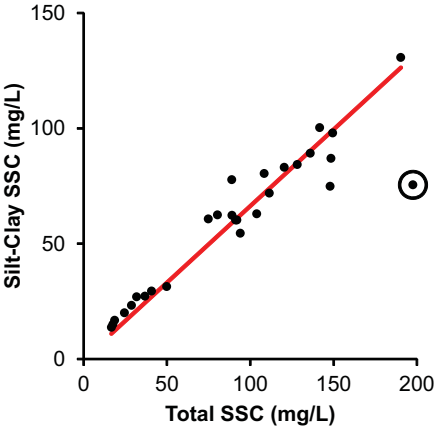


**Figure 6.** Relation between the total and silt-clay concentrations. The highlighted point (June 28; Profile 4) is removed in calculation of the $R^2$ value (0.93) and the regression is forced through the origin to give a slope of 0.66.

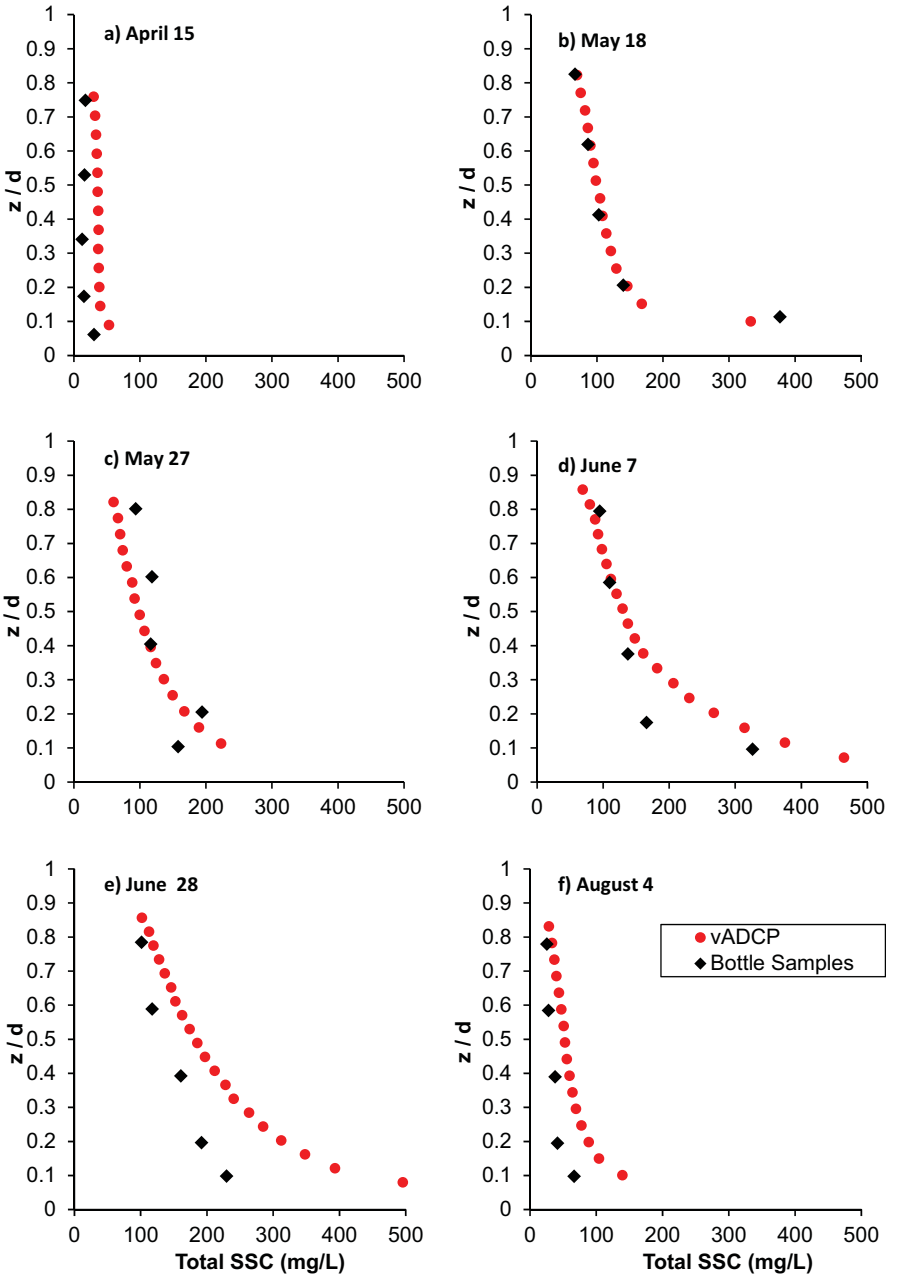


**Figure 7.** Vertical profiles of measured suspended sediment concentration from the bin × bin calibrated vADCP and corresponding bottle samples. Data from Profile 3, except 15 April and 7 June which are Profile 4 because either bottle or VADCP profiles were not available.

Initial plotting of the data reveals an excellent correlation save one errant datum (observations of 27 May: see Figure 11). We are uncertain why this datum plots off-trend, but we delete it from the calibration. Table 2 gives statistics of the beam-averaged correlation based on the backscatter data from the first 60 m of the cross-stream record collected in the five remaining measurement campaigns, and on an average of the corresponding observed *SSC* from in-beam bottle samples collected at 27.5, 50, and 55 m from the instrument. The bottle sample data were averaged as

$$c_T = \sum c_i w_i / \sum w_i \tag{11}$$

in which wi is the width of channel that each sample represents.

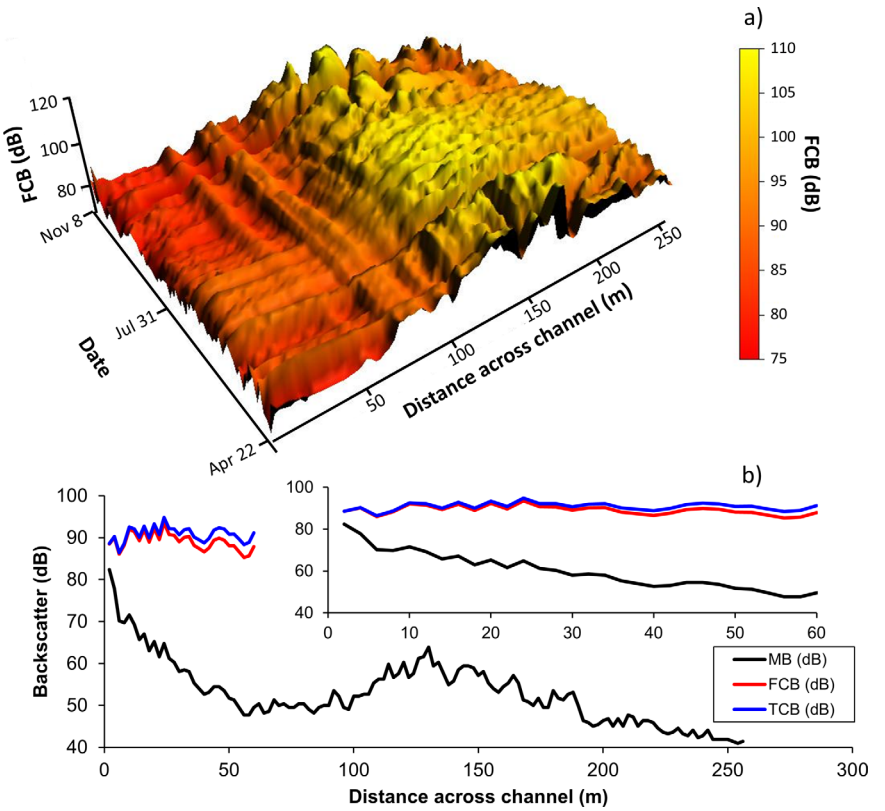


**Figure 8.** (a) Cross-stream profiles of fluid corrected backscatter (*FCB*) plotted through time. (b) Profiles of measured backscatter (MB), *FCB*, and sediment and water-corrected backscatter (*SCB*) measured on 28 June 2010. The corrected plots are truncated at 60 m. Inset: expanded view of corrected plots.

The correlations displayed in Figure 11 are very high and the gradients not significantly different than the theoretically expected value of 0.1. Silt-clay correlates very well with backscatter and clearly controls the correlation with total suspended solids. There is no coherent relation between sediment attenuation and silt-clay concentrations (Figure 12), except during peak flow (28 June) when $S_{FCB,r}$ is negative, indicating there is some attenuation of the signal at high sediment concentrations [cf. *Moore et al.*, 2013]. At lower flows, $S_{FCB,r}$ is negligibly small and varies between positive and negative values. Gradients in the *FCB* profile are due to variability in the shape of the measured profile. The result confirms initial expectations that attenuation is negligibly small—an assumption underlying the adoption of equation (9a)—so *FCB*-corrected results and *SCB*-corrected results are virtually the same (that is, removal of the residual slope has no material effect on the results). $K_t$ appears to vary between 65 and 110, the high values being for sand. The correlations are so high that no back transform correction was applied (correlation is essentially 1.0), and the functional estimate coincides with the regression equation.

## 4. Calculation of Sediment Loads

### 4.1. Bottle Samples

Sediment flux in each of the five profiles was calculated from bottle samples according to

$$q_{sj} = \sum c_i u_i d_i \tag{12}$$

in which j indexes a profile, and for the channel as

$$Q_s = \sum q_{sj} w_j \tag{13}$$

Details of the analysis of the bottle samples for sediment flux estimation are given in *Attard et al.* [2014].

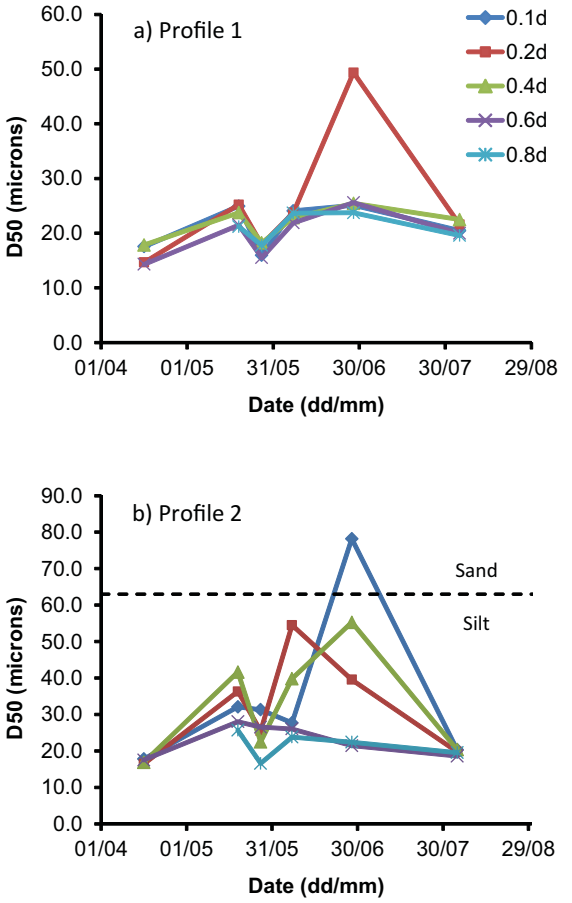


**Figure 9.** Profiles of suspended sediment grain size ($D_{50}$) on Profiles 1 and 2, through the season. The point for 30.06 at 0.2*d* on Profile 1 (in true beam) may be spurious, but points on Profile 2 (in the contaminated beam) indicate that significant excursions in sediment grain size do occur. Data in *Attard et al.* [2014, Figure 8]; 0.1d is near the bed and 0.8d is near the water surface.

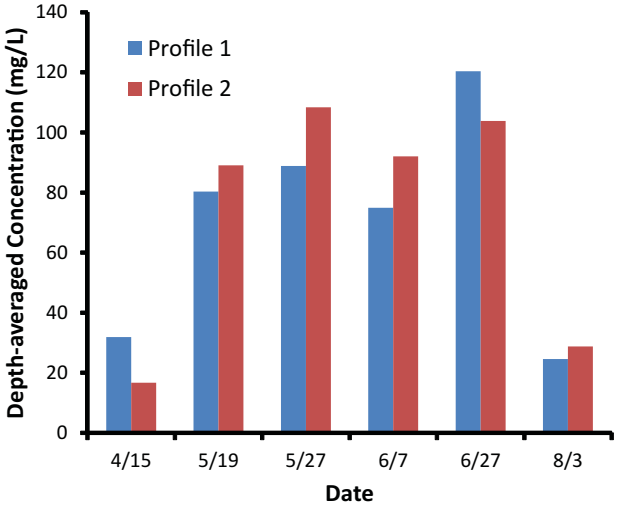


**Figure 10.** Comparison of profile-average suspended sediment concentration at Profiles 1 and 2, from bottle sampling.

### 4.2. Comparison of Flux Estimates: 600 kHz Vertical ADCP

The sediment flux was estimated from the vADCP measurements using equations (12) and (13), but $c_i$ was derived from the vADCP bin-by-bin calibration. Using the depth-averaged calibration, sediment flux was also calculated for each profile from

$$<q_{sj}> = <SSC_j><u_j> d_j \quad (14)$$

wherein <u> is the depth-averaged velocity. Sediment flux for the channel is then

$$Q_s = \sum <q_{sj}> w_j \quad (15)$$

Figure 13 compares SSC estimates derived from the bin-by-bin vADCP calibration (Figure 5). The correspondence is good but shows some significant underestimates at low to moderate sediment concentrations. Comparison with depth-averaged sediment fluxes, also shown in Figure 13, shows generally superior precision, but some significant overestimates on the high flow dates. The biased results can be traced to variation about the mean calibration relations (Figure 5), effects of which are also displayed in Figure 7.

### 4.3. Comparison of Flux Estimates: 300 kHz Horizontal ADCP

In order to calculate suspended sediment flux in the channel from continuous hADCP records, we must establish a correlation between the beam-averaged calibration based on measurements in the beam, reported in Table 2, and some measure of sediment flux in the entire channel. We have explored two ways of accomplishing this:

1. We correlate the sediment flux in the channel (determined from integration of the bottle samples) with flux through the ensonified volume. Sediment flux passing through the acoustic cone of the hADCP is estimated as

$$Q_{sh} = SSC_h < u_h > A_c \quad (16)$$

wherein $SSC_h$ is the suspended sediment concentration obtained from the beam-averaged calibration, $<u_h>$ is the mean velocity of the water column, averaged along the beam, and $A_c$ is the 2-D cross section of the acoustic beam

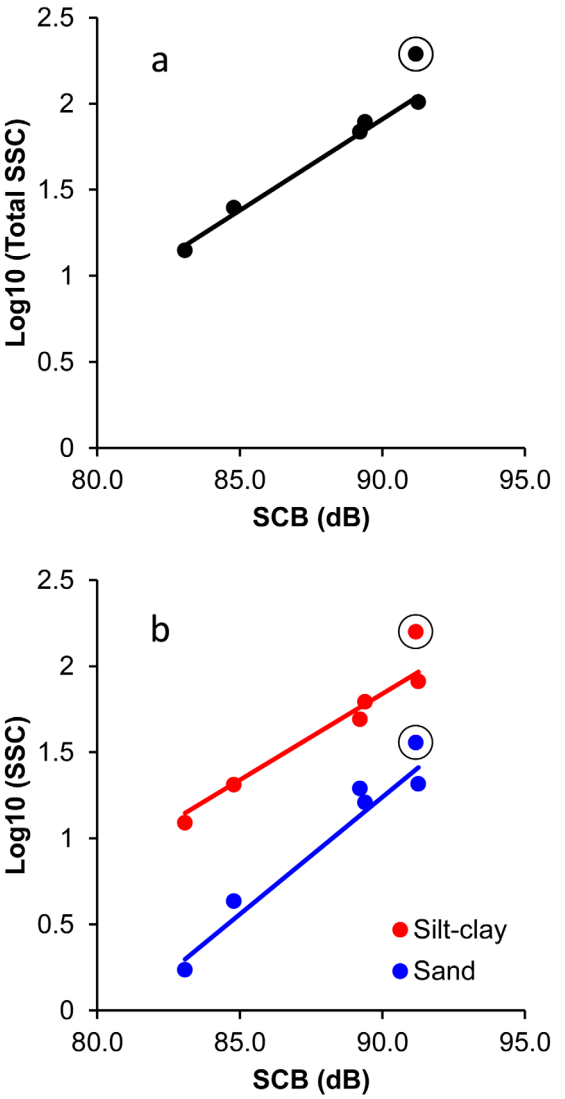


**Figure 11.** Along-beam-averaged hADCP calibration curves between sediment corrected backscatter (SCB) and (a) total suspended sediment concentration (SSC) and (b) sand and silt concentration. Lines are regression equations: further details in text. Because of interference, the acoustic profiles are truncated at 60 m. The circled point is the errant datum from 27 May.

$$A_c = \frac{1}{2}\left(30 \text{ bins} * \frac{2\text{m}}{\text{bin}}\right) h_b \quad (17)$$

wherein $h_b$ is the height of acoustic beam at 60 m and 2 m/bin denotes the 2 m width of a bin. Using this estimate, we develop a correlation between $Q_{sh}$ and sediment flux in the channel based on bottle sample vertical profiles, $Q_{sChan}$, that has the form

$$Q_{sChan} = aQ_{sh}{}^{b} \quad (18)$$

where a and b are derived from least squares regression.

2. We relate channel-averaged *SSC* to *SSC* in the ensonified area. A correlation is established between $SSC_h$ and the measured channel-averaged suspended sediment concentration, $SSC_{Chan}$, that has the form

$$SSC_{Chan} = aSSC_h{}^{b} \quad (19a)$$

in which *a* and *b* are, again, derived from least squares regression. Sediment flux is then calculated as

$$Q_{sChan} = SSC_{Chan} * Q \quad (19b)$$

wherein $Q$ is the discharge from the WSC gauging station at Mission. In a relation similar to that of equation (19a), we also study the correlation between $SSC_h$ and $SSC_{p3}$, the depth-averaged suspended sediment concentration at Profile 3 (Figure 2), a central profile formerly used by the Water Survey of Canada to obtain single-vertical bottle samples as an index of suspended sediment flux in the river. In each case, we examine relations for total *SSC*, sand, and silt/clay.

In deriving both $Q_{sh}$ and $SSC_h$, we use summary mean values directly derived from

**Table 2.** Summary of hADCP Calibrations

| | *n* | Slope (*a*) | Intercept (*b*) | $R^2$ | *P* Value[a] | SEE[b] | Confidence Range of Slope[c] |
|---|---|---|---|---|---|---|---|
| *30 Bins: FCB* | | | | | | | |
| Full GSD | 5 | 0.098[d] | −6.89 | 0.99 | $2.82 \times 10^{-04}$ | 0.037 | 0.082–0.113 |
| Sand | 5 | 0.125[d] | −10.0 | 0.95 | $4.64 \times 10^{-03}$ | 0.123 | 0.073–0.177 |
| Silt-clay | 5 | 0.092[d] | −6.46 | 0.99 | $2.89 \times 10^{-04}$ | 0.035 | 0.077–0.107 |
| *30 Bins: SCB* | | | | | | | |
| Full GSD | 5 | 0.106[d] | −7.63 | 0.99 | $4.50 \times 10^{-04}$ | 0.043 | 0.086–0.126 |
| Sand | 5 | 0.136[d] | −11.0 | 0.95 | $4.81 \times 10^{-03}$ | 0.124 | 0.079–0.193 |
| Silt-clay | 5 | 0.100[d] | −7.16 | 0.99 | $4.93 \times 10^{-04}$ | 0.042 | 0.080–0.119 |

[a]For regression slope.
[b]Standard error of estimate: $\log_{10}$ units.
[c]The 95% range.
[d]Not significantly different than 0.100 ($p = 0.05$).

beam-average quantities, hence covariance issues (between flow and sediment concentration) do not arise. We employ regression since the results will be used for prediction. Either method can be used to predict a continuous record of sediment flux from the hADCP data. We seek to learn whether beam-average results yield unbiased estimates of the load. (The regression equation may, of course, offset systematic bias between the two estimates provided that bias is consistent across the range of values.) We conducted the analysis using *SCB* corrected data. The regressions described in equations (18) and (19b) were established for the full grain-size distribution and for the load components in log linear form (Figure 14). Table 3 summarizes the parameters of these relations. In Table 3, we give parameters for the median regressions: that is the back-transformed power relations without transform bias correction. This form discounts the effect of excentric outliers (here particularly, the high flow points) and is adopted because of the irregular distribution of the small data sets.

The correlations for the full-channel sediment flux, illustrated in Figure 14, are all strong, most $R^2$ values being around 0.90 or above for the full grain-size distribution (Table 3). However, the full-channel correlations for sand in *SSC*-derived relations fall to 0.80. The small number of data points ($n = 6$) means that the analyses have low statistical power so that standard errors of the regression coefficients are large. However, all regression slopes for the full-channel actually cluster around the value 1.0. The value 1.0 implies simple proportional relations between sediment load and concentration in the hADCP beam and in the river, the proportional ratio being the intercept of the relation. On this basis, $Q_s \approx 170\ Q_{sh}$ for the full range of suspended sediment, while $Q_{s\text{-}sand} \approx 300 Q_{sh\text{-}sand}$ and $Q_{s\text{-}silt.clay} \approx 140 Q_{sh\text{-}silt/clay}$.

The proportional relations based on *SSC* are close to 2.0, except sand rises to 2.34, as one would expect since most sand suspension occurs in the unensonified main flow. The correlation of $SSC_h$ with $SSC_{p3}$ ($n = 5$) returns $R^2 \approx 0.75$ and regression slopes fall near 0.75 (though no result can be confidently declared to be statistically different than 1.0). In this case, there is no simple proportionality between hADCP values and those at P3. This is not surprising as P3, in the thalweg, is subject to relatively high sediment concentrations all season, reflected in larger coefficients but a less rapid rate of adjustment with increasing flow than in the equivalent full-channel comparisons.

All the results are unbiased (Figure 15) and, apart from one set of underpredictions for total grain-size distribution and sand deriving from an excentric high flow datum (Figure 14), relatively precise.

### 4.4. The Sediment Flux Regime

Figure 16 reveals that the annual sedigraph exhibits hysteresis, with higher sediment concentration and, therefore, sediment flux on the rising limb than on the falling limb. This feature of the annual sediment load is well known [*McLean et al.*, 1999; *Attard et al.*, 2014], so the result confirms that the measurements using ADCP data capture an important detail of the annual sediment load. However, the hADCP estimates predict greater flux on the rising limb of the seasonal flood than indicated by the physical samples while at the peak flow and on the falling limb the reverse occurs. This results in greater hysteresis than is displayed by the physical samples. In comparison, the vADCP estimates of sediment transport, sampled in the same positions as the bottle samples, show greater congruence with the physical samples and lesser hysteresis.

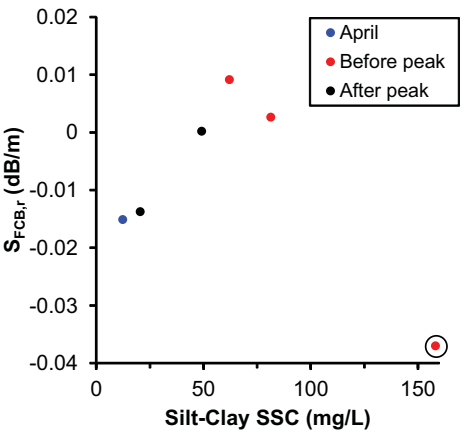


**Figure 12.** Data of sediment attenuation versus silt-clay concentration for the hADCP; the circled point is from 28 June measurements.

## 5. Discussion

### 5.1. Can we Directly Calibrate Conventional Bottle Sample Field Measurements of SSC Against Acoustic Signals?

The sensitivity of acoustic signals to suspended sediment concentration has been demonstrated in several rivers [e.g., *Wall et al.*, 2006; *Topping et al.*, 2007; *Wright et al.*, 2010; *Moore et al.*, 2011, 2013; *Sassi et al.*, 2012; *Wood and Teasdale*, 2013], in

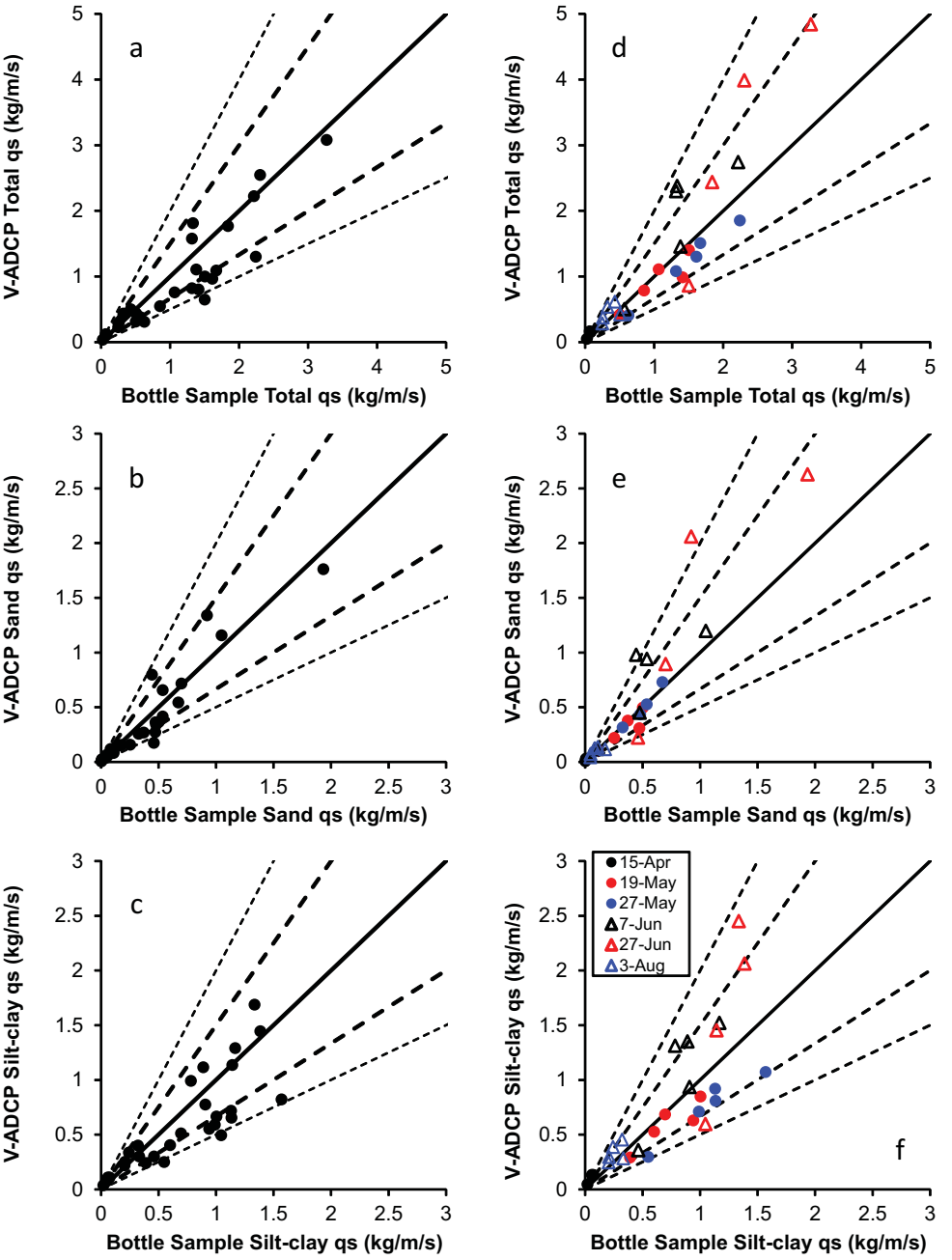


**Figure 13.** Comparison of vADCP bin-by-bin calibrated (a–c) and depth-averaged (d–f) sediment fluxes. Figures 13a and 13d are for total suspended sediment concentration, Figures 13b and 13e are for suspended sand concentration, and Figures 13c and 13f are for silt-clay concentration. The thick dashed lines are ±50% and the thin dashed lines are ±100%.

conditions both of a high silt/clay load and a low overall load. In comparison, the silt/clay load in Fraser River is modest, and the preponderance is silt, while the overall load peaks at an intermediate level due to the entrainment of sand from the bed in the higher flows. Our tests have been conducted in a substantially different environment than previous investigations and so contribute to a robust evaluation of how widely the method might be employed.

*Topping et al.* [2007] and *Wright et al.* [2010] contrasted the response of fine (silt-clay) and coarse (sand) suspended material to acoustic energy, noting that fines dominantly attenuate the reflected signal while coarse material scatters acoustic energy. Accordingly, they suggested that suspended silt and clay

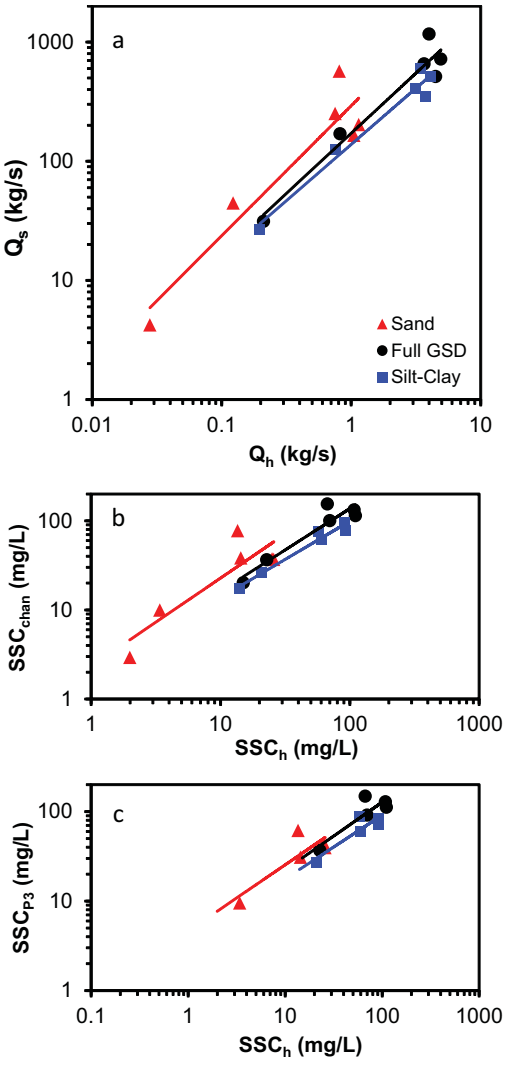


**Figure 14.** (a) Relations between sediment flux in the 300 kHz hADCP cone derived from the sediment corrected backscatter calibration ($Q_h$) and sediment flux in the channel ($Q_s$), (b) SSC in the 300 kHz hADCP cone ($SSC_h$) and SSC in the channel ($SSC_{chan}$), and (c) $SSC_h$ and SSC at Profile 3 ($SSC_{P3}$).

concentration be measured via acoustic signal attenuation, while sand can be measured via acoustic backscatter. It has been suggested [*Topping et al.*, 2007] that this division should remain valid for suspended sediment concentration varying from 10 to $10^4$ mg $L^{-1}$. In this light, our relation of silt-clay to backscatter appears unusual, though not without precedent, and perhaps related to the dominantly coarse silt makeup of the load and its relation to attenuation properties of our instruments (Figure 3). Considering backscatter, at 300 kHz response at 20 μm (see Figure 9 for grain size) is an order of magnitude less effective than at 200 μm. However, similar results (that is, good correlation of silt-clay with *SCB*) have previously been obtained in Snake and Clearwater Rivers using 1.5 and 3.0 MHz hADCPs [*Wood and Teasdale*, 2013] and the coefficients obtained in their equations are similar to those we have obtained. Our calibrations for total *SSC* and for sand concentration are highly significant but in view of the dominance of silt in the suspended load of the river, the calibration of total *SSC* mainly depends on the coherent relation obtained for silt-clay.

The bin-by-bin correlation derived from the vADCP is slightly poorer than the averaged results, possibly being degraded by variation due to the imperfect collocation of samples and the ADCP profiles, but also by the significant variation in grain size and concentration in the vertical profile. While the slope of the sand relation approximately conforms with theory, the slopes for total *SSC* and silt-clay depart from the theoretically expected value of 0.1. The beam-averaged procedure yields the more robust results. Bin-by-bin correlation must contend with the possibility that the grain size of suspended sediment may vary from bin to bin in a systematic way, which may contribute a portion of variance to the

**Table 3.** Summary of SCB-Corrected hADCP Correlations Plotted in Figure 14

| Relation | *n* | Intercept (*a*)[a] | Slope (*b*) | $R^2$ | *P* Value | Confidence Range of Slope | Std. Error of Estimate |
|---|---|---|---|---|---|---|---|
| *Full GSD* | | | | | | | |
| $Q_s = aQ_h^b$ | 6 | 172 | 1.01[b] | 0.94 | $1.4 \times 10^{-3}$ | 0.66–1.36 | −30 to +44% |
| $SSC_{Chan} = aSSC_h^b$ | 6 | 1.92 | 0.93[b] | 0.89 | $4.4 \times 10^{-3}$ | 0.48–1.37 | −26 to +35 |
| $SSC_{P3} = aSSC_h^b$ | 5 | 3.92 | 0.76[b] | 0.78 | $4.9 \times 10^{-2}$ | 0.01–1.51 | −26 to +35 |
| *Sand* | | | | | | | |
| $Q_s = aQ_h^b$ | 6 | 292 | 1.09[b] | 0.89 | $5.2 \times 10^{-3}$ | 0.54–1.64 | −48 to +94% |
| $SSC_{Chan} = aSSC_h^b$ | 6 | 2.34 | 0.99[b] | 0.79 | $1.8 \times 10^{-2}$ | 0.28–1.70 | −46 to +85 |
| $SSC_{P3} = aSSC_h^b$ | 5 | 4.63 | 0.74[b] | 0.73 | $6.6 \times 10^{-2}$ | −0.09–1.57 | −35 to +54 |
| *Silt/Clay* | | | | | | | |
| $Q_s = aQ_h^b$ | 6 | 138 | 0.94[b] | 0.97 | $4.2 \times 10^{-4}$ | 0.70–1.19 | −21 to +27% |
| $SSC_{Chan} = aSSC_h^b$ | 6 | 1.91 | 0.86[b] | 0.96 | $5.0 \times 10^{-4}$ | 0.62–1.09 | −14 to +16 |
| $SSC_{P3} = aSSC_h^b$ | 5 | 3.44 | 0.71[b] | 0.82 | $3.4 \times 10^{-2}$ | 0.10–1.32 | −21 to +26 |

[a]Intercept is back-transformed from the log linear form without bias correction: this gives the "median regression," which is robust against excentric outliers. We have adopted these results because the distribution of the data is irregular. Range of regression slope is based on the 95% confidence interval.

[b]Not significantly different than 1.0 ($p = 0.05$).

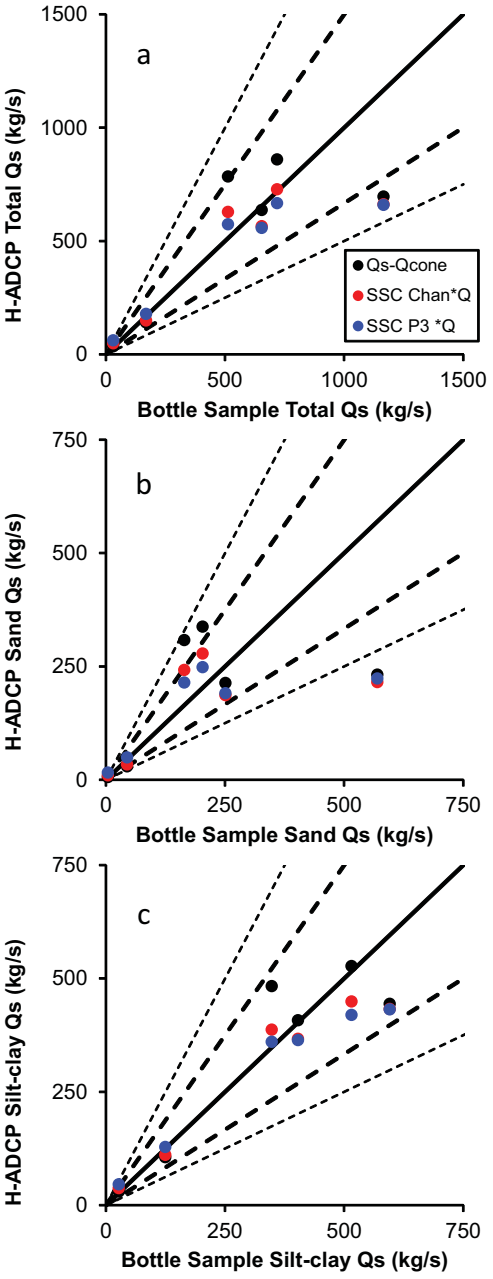


**Figure 15.** Comparison of sediment flux *Qs* measured by bottle sampling and the calibrated 300 kHz hADCP. The thick dashed lines are ±50% and the thin dashed lines are ±100%.

calibration relation. Beam-averaged calibration avoids this possibility, but not the related possibility that the entire population of suspended sediment in the water column might, over time, change in a way that affects its backscatter and/or attenuation effects, hence the entire calibration. This may happen within a short period as suspended sediment load varies with flow and might, again, bias a calibration.

There is, indeed, the appearance of seasonal drift in the vADCP calibrations that we infer—consistent with the constraints posed by the sonar equation—to be associated with the changing character of the suspended sediments. If we group low flow and postfreshet data, the slopes of the prefreshet and postfreshet instrument calibrations are essentially the same, but the grain-size-dependent constant ($K_t$) changes. It is possible that both the calibration slope and $K_t$ change over the season. If this phenomenon is general [see also *Sassi et al.*, 2012], it will greatly handicap estimation of suspended sediment load in association with routine ADCP measurements of streamflow. These calibrations can, then, be viewed only as empirical results, the continuing validity of which will depend on consistency in the makeup of the suspended sediment load in the river. There remains the possibility that in rivers with a strong and consistent flow-related hysteresis in grain size, separate calibrations for the rising and falling limb of hydrographs may produce stable calibrations, but it is not possible to assess this with our limited data set.

The beam-averaged correlations for the hADCP are very high. The slope of the relation for the full sediment load is not significantly different than the theoretically predicted value of 0.1, but that for the sand load exceeds that value by 25–35%, presumably, again, because of grain-size variation. The season-long consistency of these results may be the consequence of the consistency of suspended sediment size in the nearshore ensonified zone (Figure 9), but it remains remarkable that the correlation with the backscatter signal is so coherent, given the even greater dominance of silt in that zone than in the channel as a whole.

In sum, our results suggest that both the 300 and 600 kHz instruments are sensitive to suspended sediment. In particular, we are able to obtain linear relations between the logarithm of SSC and acoustic backscatter for the full grain-size distribution and for two components of the load. However, it should be recognized that that determination of one or other of these components is redundant inasmuch as their sum constitutes the total load. That we were able to achieve the hADCP calibrations with only five data points (one clearly aberrant point being ignored) suggests that random sources of variation are not strong. Clearly, however, the possibility for calibration drift requires further investigation.

The respective agreement and deviations from theoretical expectations between the 300 and 600 kHz instruments raise the question of whether the seasonal drift we observe is due to the lack of a suitable sediment attenuation correction for the vADCP. This is certainly possible, but unlikely. Theoretical attenuation

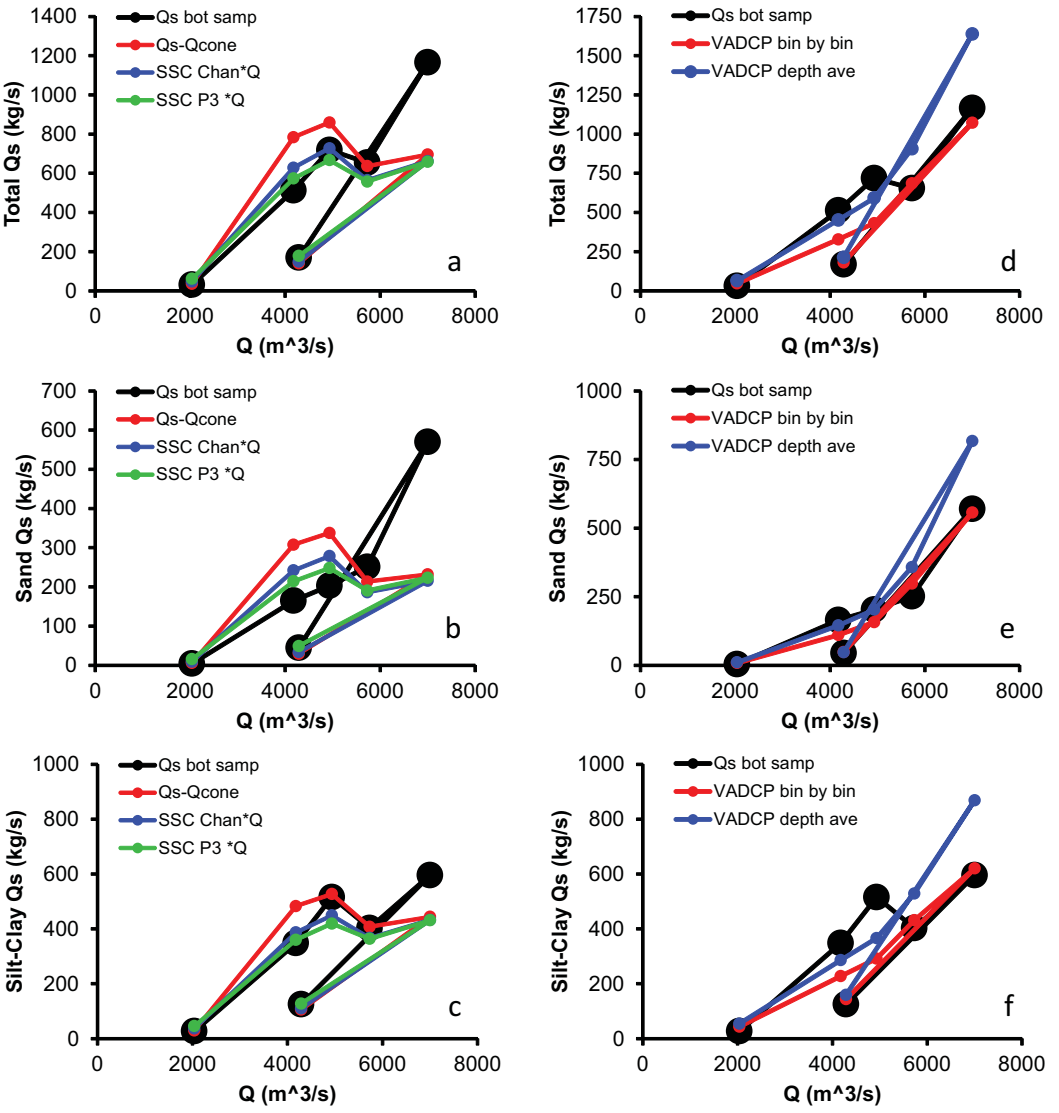


**Figure 16.** Measured ($Q_s$ bottle samples) and predicted hysteresis curves using the (a–c) 300 kHz hADCP and (d–f) the 600 kHz vADCP for the (a, d) total sediment load, (b, e) sand load, and (c, f) silt-clay load. Only the sediment corrected calibrations are used. The hysteresis proceeds in clockwise order.

coefficients (Figure 3) for our instrument frequency, sediment size, and mass concentration should be small ($10^{-2}$–$10^{-3}$ dB/m) owing to the gap between viscous and scattering sediment attenuation centered at ~35 μm (Figure 3). The contribution of the sum of viscous and scattering attenuation to the variation in *FCB* over the range (~10 m depth) would be <3% at high flows and <0.1% at low flows. Therefore, the attenuation is negligible for our conditions. It is possible that a more rigorous application of acoustic theory to our data could eliminate the seasonal drift we observe, but that would require frequent observations of mass concentration, grain size and its distribution, which would largely eliminate the need for hydroacoustic sediment observations.

### 5.2. What Is the Most Appropriate Methodology to Calculate Sediment Loads From a Calibrated ADCP?

Acoustic measurements are relatively easily taken and appear to retain essentially all of the variability contained in traditional physical measurements. However, while vADCP results may be integrated up to estimate total suspended sediment flux in much the same manner that one integrates physical bottle samples, the hADCP results, integrated up for the entire sampled volume, remain index results only since only the

ensonified volume of water along the beam is directly sampled. Hence, there must still be an ancillary correlation between the acoustic measurement and some sample that is considered to fairly represent the suspended sediment load in the channel. Direct correlations between characteristics of hADCP acoustic beams and depth-integrated sediment samples lump the acoustic calibration and the index correlation together. We have separated the two relations in our hADCP methods, providing an opportunity to assess acoustic calibration and index correlation separately.

In light of this, it is useful to assess how well the vADCP and hADCP surrogate measurements reproduce the pattern and magnitude of sediment flux in the Fraser River. There are two components of the pattern that need to be reproduced by the ADCP measurements—the seasonal increase and decrease in sediment concentration and the associated hysteresis that occurs in *SSC* [*McLean et al*., 1999; *Attard et al*., 2014]. Figure 16 indicates that the seasonal effect is captured by both the vADCP and the hADCP, regardless of the index correlation method used to calculate the sediment flux from the hADCP. It appears, however, that the hADCP results are first positively, then negatively biased through the season in comparison with physical samples taken across the full channel. Sediment dynamics in the ensonified area—a nearshore area of relatively quiescent flow—in comparison with those for the channel as a whole can produce such an effect. The vADCP appears to predict the magnitude of flux and shape of the hysteresis better than the hADCP. The depth-averaged vADCP flux correctly maps the shape of the hysteresis, but the magnitude of sediment flux at high flow is missed. The bin-by-bin correlation better matches the high flow measured flux, but underpredicts moderate flow sediment flux on the rising limb of the hydrograph, missing the shape of the hysteresis.

On the basis of the calibrations, however, the hADCP performs with better precision in direct prediction of sediment flux in the beam. In principle, the instrument has several distinct advantages over the vADCP and at-a-point instruments. The hADCP measurements can be acquired continuously, hence preserving as direct measurements the full range of temporal variability. The hADCP signals can also be selected to vary the range of spatial integration, from minimum bin size out to the full range of the instrument (provided interference from the bed, the water surface or structures be avoided). Hence both spatial and temporal variability can be recovered with far higher resolution than any prior measurement technique has achieved. But current instruments do not sample the entire width of large rivers so that the auxiliary correlation remains necessary.

The method of correlation used to link the hADCP index of sediment flux to sediment flux in the channel matters. For the full GSD, all the methods predict sediment flux and the result is generally within ~50% of the actual sediment flux (Figure 15): since the relations are unbiased, integration over time will yield results with much lower variance. The peak flow measurement sits above the index correlation curve (Figure 14), which results in underprediction of sediment flux from the hADCP (Figure 15). This affects both the magnitude and pattern of hysteresis. While the accuracy of the index correlation appears to matter, there is little to recommend one correlation method over another. All index correlations appear to produce similar results (Figures 14–16).

## 6. Conclusions

We conclude from the strength of our calibration exercises that there is a firm basis for inferring SSC and suspended sand concentrations on a continuous basis from hADCP measurements. It appears, however, that empirical elements of the calibration in field conditions dictate that the maintenance of a consistent calibration depends on consistency in the makeup of the suspended sediment flux in the river. Accordingly, vADCP measurements appear to be particularly exposed to calibration drift that might also affect hADCP measurements, depending on suspended sediment dynamics in the ensonified field.

In this paper, we have, then, confirmed that

i. vADCP measurements reliably assess suspended sediment concentration in the water column, but purely empirical calibration remains subject to variations in the size of suspended sediments;
ii. Profile-averaged calibrations are more consistent with theoretical expectations than bin-by-bin calibrations;
iii. Silt content in moderate concentration calibrates to the acoustic backscatter signal;

iv. Empirical hADCP calibrations are robust and conform with sonar theory so long as suspended sediment size distribution remains relatively consistent;
v. Auxiliary index correlations can be derived to support hADCP sediment flux measurements, but they must accurately represent a wide range flows;
vi. Sediment-associated beam attenuation appears to be negligible at concentrations below 150 mg $L^{-1}$ (our overall mean suspended sediment concentration) for our conditions.

These results hold the promise that ADCP measurements may be adaptable for routine measurement of suspended sediment flux in rivers.

**Acknowledgments**
We thank Russell White and Bruno Tassone from the Water Survey of Canada, Environment Canada for providing funding for the project. Emily Huxter, Curt Naumann, and WSC staff provided technical support, including water discharge measurements during our sampling campaigns. Megan Hendershot, Sally Haggerstone, and Jessica Fickell provided technical support for the sediment sampling operation and sample/data analysis. A perceptive review by A. J. F. Hoitink prompted us to give increased attention to considerations of acoustic theory and the empirical nature of our measurements. M.A. was supported by a SFU Graduate Fellowship and Discovery grants from the Natural Sciences and Engineering Research Council of Canada to J.V. and M.C. All summary data related to this article are presented in the paper and may be obtained from the senior author.

## References

Attard, M. E., J. G. Venditti, and M. Church (2014), Suspended sediment transport in the Lower Fraser River, British Columbia, *Can. Water Resour. J.*, *39*, 356–371.
Bradley, R. W., J. G. Venditti, R. A. Kostaschuk, M. Church, M. Hendershot, and M. A. Allison (2013), Flow and sediment suspension events over low-angle dunes: Fraser Estuary, Canada, *J. Geophys. Res. Earth Surf.*, *118*, 1693–1709, doi:10.1002/jgrf.20118.
Buschman, F. A., A. J. F. Hoitink, S. M. de Jong, P. Hoekstra, H. Hidayat, and M. G. Sassi (2012), Suspended sediment load in the tidal zone of an Indonesian river, *Hydrol. Earth Syst. Sci.*, *16*, 4191–4204.
Crawford, A. M., and A. E. Hay (1993), Determining suspended sand size and concentration from multifrequency acoustic backscatter, *J. Acoust. Soc. Am.*, *94*(6), 3312–3324.
Defendi, V., V. Kovacèvić, F. Arena, and L. Zaggia (2010), Estimating sediment transport from acoustic measurements in the Venice Lagoon inlets, *Cont. Shelf Res.*, *30*, 883–893.
Deines, K. L. (1999), Backscatter estimation using broadband acoustic Doppler current profilers, in *Current Measurement, 1999*, Proc. IEEE 6th Working Conf., pp. 249–253. IEEE, N. Y.
Downing, J. P. (1983), An optical instrument for monitoring suspended particles in ocean and laboratory, in *Proceedings of OCEANS 1983*, pp. 199–202, IEEE, N. Y.
Duan, N. (1983), Smearing estimate: A nonparametric retransformation method, *J. Am. Stat. Assoc.*, *78*, 605–610.
Filizola, N., and J. L. Guyot (2004), The use of Doppler technology for suspended sediment discharge determination in the River Amazon, *Hydrol. Sci. J.*, *49*, 143–153.
Flammer, G. H. (1962), Ultrasonic measurement of suspended sediment, *U.S. Geol. Surv. Bull.*, *1141-A*, 48 pp.
Gartner, J. W. (2004), Estimating suspended solids concentrations from backscatter intensity measured by acoustic Doppler current profiler in San Francisco Bay, California, *Mar. Geol.*, *211*, 169–187.
Gray, J. R., and M. N. Landers (2013), Measuring suspended sediment, in *Comprehensive Water Quality and Purification*, vol. 1, pp. 157–204, edited by S. Ahuja, Elsevier, Amsterdam.
Guerrero, M., R. N. Szupiany, and F. Latosinski (2013), Multi-frequency acoustics for suspended sediment studies: An application in the Parana River, *J. Hydraul. Res.*, *51*, 696–707.
Hamilton, L. J., Z. Shi, and S. Y. Zhang (1998), Acoustic backscatter measurements of estuarine suspended cohesive sediment concentration profiles, *J. Coastal Res.*, *14*, 1213–1224.
Hanes, D. M. (2013), Erratum to "On the possibility of single-frequency acoustic measurement of sand and clay concentrations in uniform suspensions" [*Cont. Shelf Res.*, *46*, 64–66], *54*, 117–118.
Hay, A. E. (1991), Sound scattering from a particle-laden, turbulent jet, *J. Acoust. Soc. Am.*, *90*, 2055–2074.
Hay, A. E., and J. Sheng (1992), Vertical profiles of suspended sand concentration and size from multifrequency acoustic backscatter, *J. Geophys. Res.*, *97*, 15,661–15,677.
Hill, D. C., S. E. Jones, and J. Prandle (2003), Derivation of sediment resuspension rates from acoustic backscatter time-series in tidal waters, *Cont. Shelf Res.*, *23*, 19–40.
Hoitink, A. J. F., and P. Hoekstra (2005), Observations of suspended sediment from ADCP and OBS measurements in a mud-dominated environment, *Coastal Eng.*, *52*, 103–118.
Holdaway, G. P., P. D. Thorne, D. Flatt, S. E. Jones, and D. Prandle (1999), Comparison between ADCP and transmissometer measurements of suspended sediment concentration, *Cont. Shelf Res.*, *19*, 421–441.
Jugaru Tiron, L., J. Le Coz, M. Provansal, N. Panin, G. Raccasi, G. Dramais, and P. Dussouillez (2009), Flow and sediment processes in a cutoff meander of the Danube delta during episodic flooding, *Geomorphology*, *106*, 189–197.
Kostaschuk, R. A., J. Best, P. Villard, J. Peakall, and M. Franklin (2005), Measuring flow velocity and sediment transport with an acoustic Doppler current profiler, *Geomorphology*, *68*, 25–37.
MacDonald, I. T., C. E. Vincent, P. D. Thorne, and B. D. Moate (2013), Acoustic scattering from a suspension of flocculated sediments, *J. Geophys. Res. Oceans*, *118*, 2581–2594, doi:10.1002/jgrc.20197.
Mark, D. M., and M. Church (1977), On the misuse of regression in earth science, *Math. Geol.*, *9*, 63–75.
McLean, D. G., M. Church, and B. Tassone (1999), Sediment transport along lower Fraser River: 1. Measurements and hydraulic computations, *Water Resour. Res.*, *35*, 2533–2548.
Moate, B. D., and P. D. Thorne (2009), Measurements and inversion of acoustic scattering from suspensions having broad size distributions, *J. Acoust. Soc. Am.*, *126*, 2905–2917.
Moate, B. D., and P. D. Thorne (2013), Scattering from suspended sediments having different and mixed mineralogical compositions: Comparison of laboratory measurements and theoretical predictions, *J. Acoust. Soc. Am.*, *133*, 1320–1334.
Moore, S. A., and A. E. Hay (2009), Angular scattering of sound from solid particles in turbulent suspension, *J. Acoust. Soc. Am.*, *126*, 1046–1056.
Moore, S. A., J. LeCoz, D. Hurther, and A. Paquier (2011), On the application of horizontal ADCPs to suspended sediment transport surveys in rivers, *Cont. Shelf Res.*, *46*, 50–63.
Moore, S. A., J. LeCoz, D. Hurther, and A. Paquier (2013), Using multi-frequency acoustic attenuation to monitor grain size and concentration of suspended sediment in rivers, *J. Acoust. Soc. Am.*, *133*, 1959–1970.

Newman, M. C. (1993), Regression analysis of log-transformed data: Statistical bias and its correction, *Environ. Toxicol. Chem.*, *12*, 1129–1133.
Reichel, G., and H. P. Nachtnebel (1994), Suspended sediment monitoring in a fluvial environment: Advantages and limitations applying an acoustic Doppler current profiler, *Water Res.*, *28*, 751–761.
Sassi, M. G., A. J. F. Hoitink, and B. Vermeulen (2012), Impact of sound attenuation by suspended sediment on ADCP backscatter calibrations, *Water Resour. Res.*, *48*, W09520, doi:10.1029/2012WR012008.
Sassi, M. G., A. J. F. Hoitink, and B. Vermeulen (2013a), Quantified turbulent diffusion of suspended sediment using acoustic Doppler current profilers, *Geophys. Res. Lett.*, *40*, 5757–5763, doi:10.1002/2013GL058299.
Sassi, M. G., A. J. F. Hoitink, B. Vermeulen, and H. Hidayat (2013b), Sediment discharge division at two tidally influenced river bifurcations, *Water Resour. Res.*, *49*, 2119–2134, doi:10.1002/wrcr.20216.
Schulkin, M., and H. W. Marsh (1962), Sound absorption in sea water, *J. Acoust. Soc. Am.*, *34*, 864–865.
Shugar, D. H., R. A. Kostaschuk, J. L. Best, D. R. Parsons, S. N. Lane, O. Orfeo, and R. J. Hardy (2010), On the relationship between flow and suspended sediment transport over the crest of a sand dune, Río Paraná, Argentina, *Sedimentology*, *57*, 252–272.
Szupiany, R. N., M. L. Amsler, D. R. Parsons, and J. L. Best (2009), Morphology, flow structure, and suspended bed sediment transport at two large braid-bar confluences, *Water Resour. Res.*, *45*, W05415, doi:10.1029/2008WR007428.
Thevenot, M. M., and N. C. Kraus (1993), Comparison of acoustical and optical measurements of suspended material in the Chesapeake Estuary, *J. Mar. Environ. Eng.*, *1*, 65–79.
Thorne, P. D., and M. J. Buckingham (2004), Measurements of scattering by suspensions of irregularly shaped sand particles and comparison with a single parameter modified sphere model, *J. Acoust. Soc. Am.*, *116*, 2876–2889.
Thorne, P. D., and D. M. Hanes (2002), A review of acoustic measurements of small-scale sediment processes, *Cont. Shelf Res.*, *22*, 603–632.
Thorne, P. D., and P. J. Hardcastle (1997), Acoustic measurement of suspended sediments in turbulent currents and comparison with in-situ samples, *J. Acoust. Soc. Am.*, *101*, 2603–2614.
Thorne, P. D., and D. Hurther (2014), An overview on the use of backscattered sound for measuring suspended particle size and concentration profiles in non-cohesive inorganic sediment transport studies, *Cont. Shelf Res.*, *73*, 97–118.
Thorne, P. D., P. J. Hardcastle, and R. L. Soulsby (1993), Analysis of acoustic measurements of suspended sediments, *J. Geophys. Res.*, *98*, 899–910.
Thorne, P. D., D. Hurther, and B. D. Moate (2010), Acoustic inversions for measuring boundary layer suspended sediment processes, *J. Acoust. Soc. Am.*, *130*, 1188–1200.
Thosteson, E. D., and D. M. Hanes (1998), A simplified method for determining sediment size and concentration from multiple frequency acoustic backscatter measurements, *J. Acoust. Soc. Am.*, *104*, 820–830.
Tiron Duţu, L., M. Provansal, J. Le Coz, and F. Duţu (2014), Contrasted sediment processes and morphological adjustments in three successive cutoff meanders of the Danube delta, *Geomorphology*, *204*, 154–164.
Topping, D. J., S. A. Wright, T. S. Melis, and D. M. Rubin (2007), High-resolution measurements of suspended-sediment concentration and grain size in the Colorado River in Grand Canyon using a multi-frequency acoustic system, in *Proceedings of the 10th International Symposium on River Sedimentation*, Moscow, 1–4 August, vol. III, pp. 330–339, International Research and Training Center for Erosion and Sedimentation, Beijing.
Urick, R. J. (1975), *Principles of Underwater Sound for Engineers*, 384 pp., McGraw Hill, N. Y.
Venditti, J. G., R. P. Humphries, M. A. Allison, J. A. Nittrouer, and M. Church (2010), Morphology and dynamics of a gravel-sand transition, paper presented at the 2nd Joint Federal Interagency Sedimentation Conference, (U.S.) Advisory Committee on Water Information, Subcommittee on Hydrology and Sedimentation, Las Vegas, Nev., 27 June to 1 July. [Available at http://acwi.gov/sos/pubs/2ndJFIC.]
Wall, G. R., E. A. Nystrom, and S. Litten (2006), Use of an ADCP to compute suspended sediment discharge in the tidal Hudson River, New York, *U. S. Geol. Surv. Sci. Invest. Rep., 2006-5055*, 16 pp.
Wall, G. R., E. A. Nystrom, and S. Litten (2008), Suspended sediment transport in the freshwater reach of the Hudson River estuary in eastern New York, *Estuaries Coasts*, *31*, 542–553.
Walling, D. E. (1977), Limitations of the rating curve technique for estimating suspended sediment loads with particular reference to British rivers, in *Erosion and Solid Matter Transport in Inland Waters: Proceedings of the Paris Symposium*, *Publication 122*, pp. 34–48, Int. Assoc. of Hydrol. Sci., Wallingford, U. K.
Wargo, C. A., and R. Styles (2007), Along channel flow and sediment dynamics at North Inlet, South Carolina, *Estuarine Coastal Shelf. Sci.*, *71*, 669–682.
Wood, M. S., and G. N. Teasdale (2013), Use of surrogate technologies to estimate suspended sediment in the Clearwater River, Idaho, and Snake River, Washington, 2008-10, *U. S. Geol. Surv. Sci. Invest. Rep., 2013-5052*, 30 pp.
Wright, S. A., D. T. Topping, and C. A. Williams (2010), Discriminating silt-and-clay from suspended-sand in rivers using side-looking acoustic profilers, paper presented at 2nd Joint Federal Interagency Sedimentation Conference, (U.S.) Advisory Committee on Water Information, Subcommittee on Hydrology and Sedimentation, June, Las Vegas, Nev. [Available at http://acwi.gov/sos/pubs/2ndJFIC.]